A Simple and Practical Duty Cycle Modulated Direct Torque Control for Permanent Magnet Synchronous Motors

Feng Niu, *Member, IEEE*, Xiaoyan Huang, *Member, IEEE*, Leijiao Ge, Jian Zhang, Lijian Wu, *Senior Member, IEEE*, Yao Wang, *Member, IEEE*, Kui Li, and Youtong Fang, *Senior Member, IEEE*

***Abstract*—This paper proposes a simple and practical duty cycle modulated direct torque control (DDTC) for permanent magnet synchronous motors. The duty cycle of active vector is obtained using a duty cycle generator according to the torque error and motor speed, which can avoid the complex calculation process associated with conventional DDTC. The design details about the duty cycle generator are illustrated, and the stability of the proposed DDTC is analyzed, which ensures the reliable operation of the motor system. Experimental results are presented to validate the effectiveness of the proposed DDTC. Furthermore, the comparative evaluation of the proposed DDTC and conventional DDTC is conducted to verify the superiority of the proposed DDTC.**

***Index Terms*—Direct torque control (DTC), duty cycle modulation (DCM), permanent magnet synchronous motor (PMSM), PI regulator.**

I. Introduction

DIRECT torque control (DTC) has become one of the most popular strategies for motor control since it was first proposed several decades ago [1]–[2]. DTC owns the advantages

Manuscript received November 12, 2017; revised February 20, 2018; accepted April 24, 2018. Date of publication May 6, 2018; date of current version December 7, 2018. This work was supported in part by the National Natural Science Foundation of China under Grant 51707174, in part by the National Postdoctoral Program for Innovative Talents under Grant BX201600132, and in part by the Research Project of Science and Technology of Hebei Province under Grant QN2016193. Preliminary results have been presented in the paper published in the Proceedings of 20th International Conference on Electrical Machines and Systems, Sydney, Australia, Aug. 11–14, 2017. Recommended for publication by Associate Editor B. G. Fernandes. *(Corresponding author: Xiaoyan Huang.)*

F. Niu is with the College of Electrical Engineering, Zhejiang University, Hangzhou 310027, China, and also with the State Key Laboratory of Reliability and Intelligence of Electrical Equipment, Key Laboratory of Electromagnetic Field and Electrical Apparatus Reliability of Hebei Province, Hebei University of Technology, Tianjin 300130, China (e-mail:

each control period to reduce power ripple of rectifier or torque ripple of motor. But these methods also need a certain amount of calculation to obtain the duty cycle even if they are independent from motor parameters.

Generally speaking, the conventional DDTC methods require a lot of calculations to obtain the duty cycle of active vector and rely heavily on the accuracy of motor parameters, which seriously deteriorates the efficiency and control performance of DDTC. In order to solve these problems, this paper proposes a simple and practical DDTC method for PMSM. The duty cycle of active vector is obtained through a duty cycle generator according to the torque error and motor speed, which can significantly reduce the computational burden. Experimental verification are conducted to validate the effectiveness and superiority of the proposed DDTC. The rest of this paper is organized as follows. Section II illustrates the PMSM model and overall control diagram of the proposed DDTC. The detailed structure and design process of duty cycle generator is described in Section III. Section III also includes the stability analysis of the proposed DDTC. The comparative evaluation of proposed DDTC and conventional DDTC is presented in Section IV, and Section V is the conclusion.

II. Duty Cycle Modulated DTC

A. Mathematical Model of PMSM

The state equations of a PMSM in the d–q reference frame are expressed as follows:

$$u_{sd} = R_s i_{sd} + \frac{d\psi_{sd}}{dt} - \omega_r \psi_{sq} \tag{1}$$

$$u_{sq} = R_s i_{sq} + \frac{d\psi_{sq}}{dt} + \omega_r \psi_{sd} \tag{2}$$

$$\psi_{sd} = L_d i_{sd} + \psi_f \tag{3}$$

$$\psi_{sq} = L_q i_{sq} \tag{4}$$

where L_d, L_q are the d-, q-axes inductances, respectively; ψ_{sd}, ψ_{sq} are the d-, q-axes flux, respectively; u_{sd}, u_{sq} are the d-, q-axes stator voltages, respectively; i_{sd}, i_{sq} are the d-, q-axes stator currents, respectively; R_s is the stator winding resistance; ψ_f is the permanent magnet flux linkage, and ω_r is the electrical rotor speed. The electromagnetic torque is expressed as

$$T_e = \frac{3}{2} p(\psi_{sd} i_{sq} - \psi_{sq} i_{sd}) \tag{5}$$

where p is the number of pole pairs.

B. Overall Control Diagram

The system diagram of the proposed DDTC is shown in Fig. 1. The control algorithm is implemented in four stages: flux and torque estimation, vector selection, duty cycle generation, and vector output. The details of each stage are illustrated as follows.

1) Flux and Torque Estimation: In each control period, the flux and torque are first estimated using corresponding observers. In this paper, the observer defined by (3) and (4) is adopted to estimate the flux because of its simple structure and excellent performance. The torque estimation can then be realized through (5). In addition, the desired torque and flux are obtained according to the speed error, PI regulator, and MTPA operation principle.

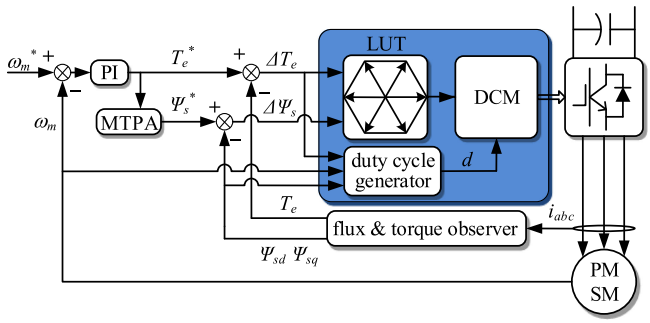

Fig. 1. System diagram of the proposed DDTC.

TABLE I
Active Vector LUT

ΔT_e	$\Delta\psi_s$	active vector
↑	↑	$u_{s(k+1)}$
↑	↓	$u_{s(k+2)}$
↓	↑	$u_{s(k-1)}$
↓	↓	$u_{s(k-2)}$

2) Vector Selection: After the estimation of flux and torque, the active vector is selected from a lookup table (LUT) according to torque error and flux error. The LUT is same with that used in DTC as shown in Table I, where ΔT_e and $\Delta\psi_s$ are torque error and flux error, respectively, k indicates that the sector flux stays in. Then, the zero vector is determined according to the selected active vector. In order to reduce the switching frequency, the active vectors u_{s1} (100), u_{s3} (010), and u_{s5} (001) are followed by zero vector u_{s0} (000), while the other three active vectors are followed by zero vector u_{s7} (111). As such, only one phase of inverter changes status in each control period.

3) Duty Cycle Generation: After the selection of optimal active vector and zero vector, the duty cycle of active vector is then obtained through a duty cycle generator. The torque error and motor speed are taken as the input of duty cycle generator, and the output is the duty cycle of active vector, which is related to the torque error and motor speed. More details about the duty cycle generator are presented in the following section.

4) Vector Output: After the duty cycle is obtained, corresponding pulsewidth modulation (PWM) signals are generated according to the vectors and duty cycle to drive the power switches of inverter. As mentioned above, the active vector is first applied to the motor, which is followed by the zero vector.

III. Duty Cycle Generator

The PMSM is a complex nonlinear system, thus it is difficult to establish an accurate mathematical model between torque variation and duty cycle of active vector, especially for interior PMSM (IPMSM) because the difference of d- and q-axes inductances makes their mathematical relationship more complex. In

order to facilitate the explanation and avoid complicated formula derivation process, this paper takes surface mounted PMSM as an example to conduct a theoretical analysis of the inner relationship between torque variation and duty cycle. For SPMSMs, the torque can be expressed as

$$T_e = \frac{3}{2} p \psi_f i_{sq}. \tag{6}$$

The derivative of torque T_e can be obtained as

$$\frac{dT_e}{dt} = \frac{3}{2} p \psi_f \frac{1}{L_q} \frac{d\psi_{sq}}{dt}. \tag{7}$$

Substitute (2) into (7) and ignore the voltage drop across stator resistance, then (7) can be rewritten as

$$\frac{dT_e}{dt} = \frac{3}{2} p \psi_f \frac{1}{L_q} (u_{sq} - \omega_r \psi_{sd}). \tag{8}$$

It can be seen from (8) that the q-axis voltage has two major functions: one is to offset the counter electromotive force caused by the rotation of d-axis flux, and the other one is to generate the required torque variation. Define the following:

$$\begin{cases} |u_{sq}| \approx d \times \frac{2}{3} U_{\rm dc} \\ d = |d_{\rm cemf} + \Delta d| \\ d_{\rm cemf} \times \frac{2}{3} U_{\rm dc} = |\omega_r| \psi_{sd} \end{cases} \tag{9}$$

where d is the duty cycle of active vector and $U_{\rm dc}$ is the dc-link voltage. Because the active vector and zero vector are already determined using the LUT shown in Table I, the duty cycle d is only related to the amplitude of selected vectors. The absolute value operations in (9) can remove the polarity of related variables. During motor operation process, the polarity of u_{sq} and ω_r are the same, thus the torque variation can be expressed as (10) according to (8) and (9)

$$\Delta T_e = \frac{p \psi_f U_{\rm dc}}{L_q} \Delta d. \tag{10}$$

It can be seen from (10) that there is a linear relationship between Δd and torque variation. When the motor operates in steady state, it can be assumed that there is no torque variation, and thus Δd is equal to 0. During the dynamic state of motor, the value of Δd is not equal to 0 anymore, and the resulting additional voltage will drive the motor to track control instructions. Because several approximate calculations are included in the above theoretical analysis process, integral operation is also necessary to obtain Δd from torque variation ΔT_e, which can reduce the error of Δd in both steady-state and dynamic operations. In addition, the error of Δd caused by saliency effect in IPMSM can also be reduced through introducing the integral operation.

According to the above theoretical analysis, the structure of duty cycle generator can be obtained as shown in Fig. 2. The input of duty cycle generator is the torque error and motor speed. The torque error is taken as the input of a PI regulator with proportional factor k_p and integral factor k_i, and then, the output of PI regulator Δd is added by $d_{\rm cemf}$ related to the motor speed according to (9). The polarity of the additional result is removed by an absolute value module, and the obtained absolute value

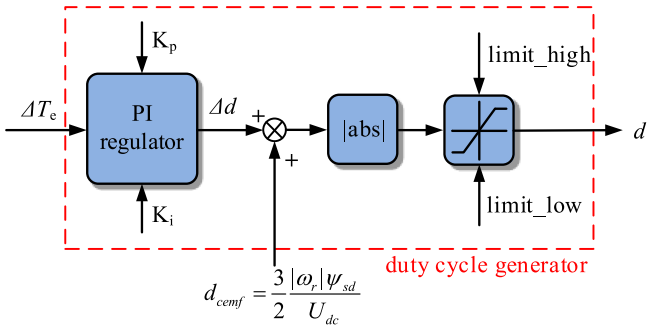

Fig. 2. Duty cycle generator.

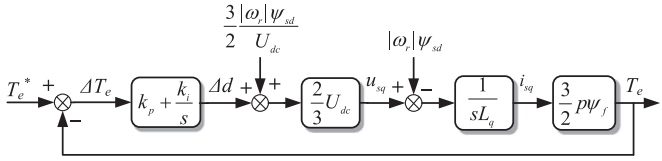

Fig. 3. Control diagram of proposed DDTC.

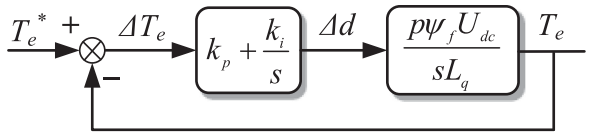

Fig. 4. Simplified control diagram of proposed DDTC.

is sent to a saturator with upper limitation (limit_high = 1) and lower limitation (limit_low = 0). Finally, the output of saturator is taken as the duty cycle d of active vector. The generator structure can ensure that the output duty cycle is limited to [0 1] to keep its rationality.

A. Proportional Factor k_p

The determination of parameters k_p and k_i for PI regulator is the key issue of proposed DDTC, which will affect the control performance in both steady-state and dynamic operations. According to (10), the proportional factor k_p can be obtained using the following:

$$k_p = \frac{L_q}{p \psi_f U_{\rm dc}}. \tag{11}$$

B. Integral Factor k_i

The values of k_p and k_i should ensure the stability of the proposed DDTC. In order to analyze the algorithm stability, the control diagram of the torque loop is established as shown in Fig. 3.

According to the simplification rules of control diagram, the control diagram in Fig. 3 can be simplified and redrawn as shown in Fig. 4.

The closed-loop transfer function of torque in Fig. 4 is

$$\frac{T_e}{T_e^*} = \frac{(k_p s + k_i) p \psi_f U_{\rm dc}}{L_q s^2 + k_p p \psi_f U_{\rm dc} s + k_i p \psi_f U_{\rm dc}}. \tag{12}$$

TABLE II
SYSTEM PARAMETERS

Motor	
Type	IPMSM
Rated power P [kW]	1
Stator resistance R [Ω]	0.8
Inductance (d-axis) L_d [mH]	5
Inductance (q-axis) L_q [mH]	10
PM flux ψ_f [Wb]	0.035
Pole pairs p	4
Inverter	
Type	2-level VSI
DC-link voltage U_{dc} [V]	100
Control	
Control period [μs]	100
K_p	7.15e-4
K_i	5e-4

Substitute (11) into (12), (12) can be rewritten as

$$\frac{T_e}{T_e^*} = \frac{L_q s + k_i p \psi_f U_{\rm dc}}{L_q s^2 + L_q s + k_i p \psi_f U_{\rm dc}}. \tag{13}$$

To ensure the stability of the torque control loop for the proposed DDTC, the root values of the denominator polynomial in (13) should be negative real number, which means that the value of k_i should meet the requirements of the following:

$$\frac{-L_q \pm \sqrt{L_q^2 - 4k_i L_q p \psi_f U_{\rm dc}}}{2L_q} < 0. \tag{14}$$

The range of k_i can be obtained through solving (14)

$$k_i > \frac{k_p}{4} = \frac{L_q}{4p\psi_f U_{\rm dc}}. \tag{15}$$

IV. EXPERIMENTAL VERIFICATION

In this section, the proposed DDTC is comparatively investigated through experimentations of a two-level VSI fed 1-kW PMSM. The main parameters of the motor system are listed in Table II. Because the comparative evaluation of DTC, MPTC, DDTC, and FOC is conducted in [9], and the comparison of different DDTC methods is conducted in [14], this paper only takes DDTC-rms method, which nominally owns the best control performance in the existing DDTC methods as stated in [14], as conventional DDTC and plays the role of benchmark in this paper.

In the experimental setup, NI PCIe-7852R module with FPGA embedded is utilized to implement the proposed and conventional DDTC control strategies. First, the simulation model, including the duty cycle generator, of the DDTC method is established and verified in MATLAB/Simulink. And then, the simulation model can be compiled and generates executable code, which can be downloaded and run in the FPGA of the NI PCIe-7852R module. In addition, the DCM module is established using NI LabVIEW and the corresponding executable code is downloaded to another FPGA controller to produce PWM signals.

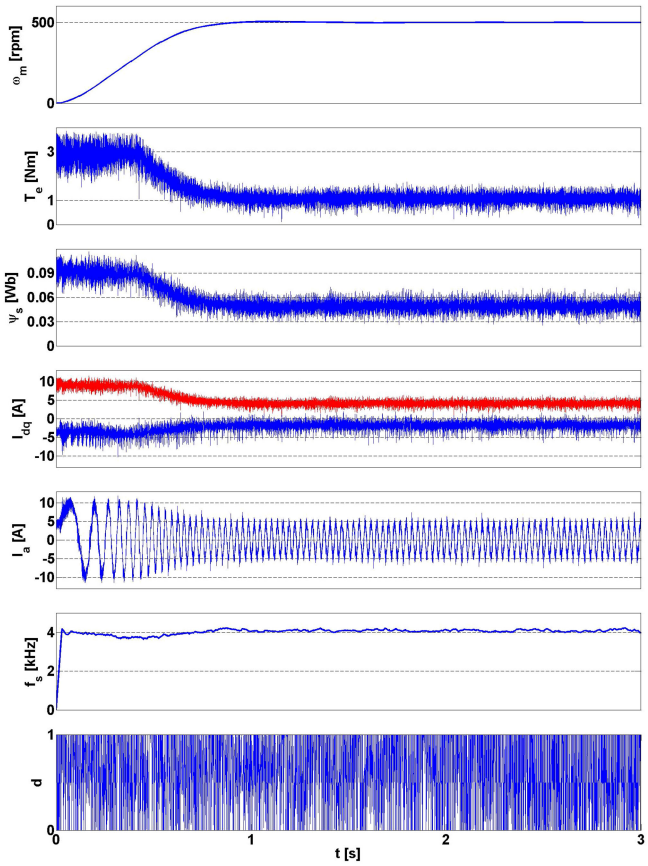

Fig. 5. Experimental results of conventional DDTC. Mechanical speed: 500 r/min, load: 1 N·m. The graphs are (from top): speed, torque, flux, d-, q-axes currents, current of phase A, switching frequency, and duty cycle.

A. Steady-State Control Performance

Figs. 5 and 6 are the experimental results of the conventional DDTC and proposed DDTC, respectively. The motor starts up to 500 r/min with 1 N·m load. It can been seen that the two DDTC methods can both quickly track the command speed while keeping their torque and flux fluctuating within a small range. From a comparative point of view, the proposed DDTC shows better control performance in terms of torque ripple level, flux ripple level, and switching frequency during both steady-state and dynamic process. It should be noted that the duty cycle of the proposed DDTC is more stable than that of conventional DDTC, which is the main reason why the proposed DDTC shows better control performance than the conventional DDTC.

Fig. 7 and 8 are the steady-state experimental results of conventional DDTC and proposed DDTC under different speeds, respectively. The experimental waveforms under various speeds are artificially spliced in one figure to highlight the impact of speed changes on control performance. Table III summarizes the quantitative index of torque ripple, flux ripple, and switching frequency, and Fig. 9 is the numerical comparison of these

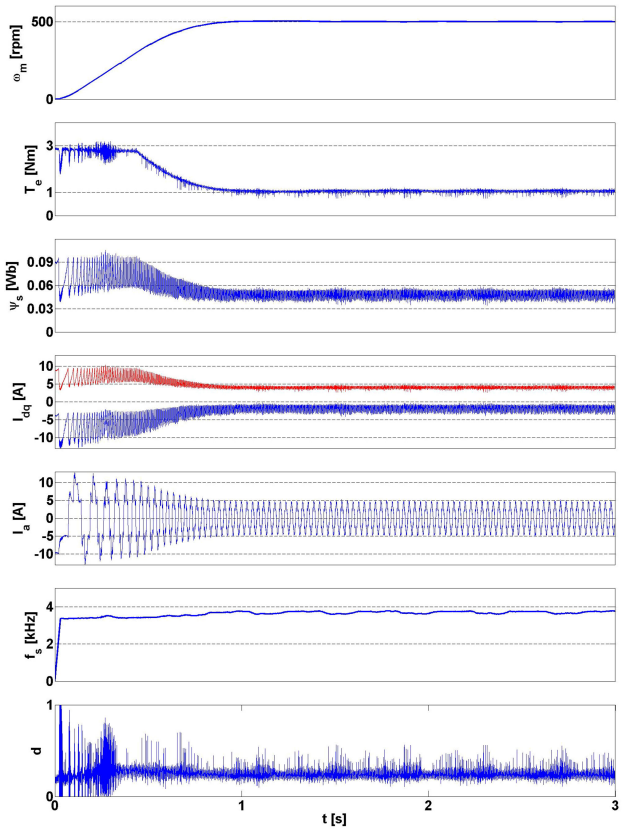

Fig. 6. Experimental results of the proposed DDTC. Mechanical speed: 500 r/min, load: 1 N·m. The graphs are (from top): speed, torque, flux, d-, q-axes currents, current of phase A, switching frequency, and duty cycle.

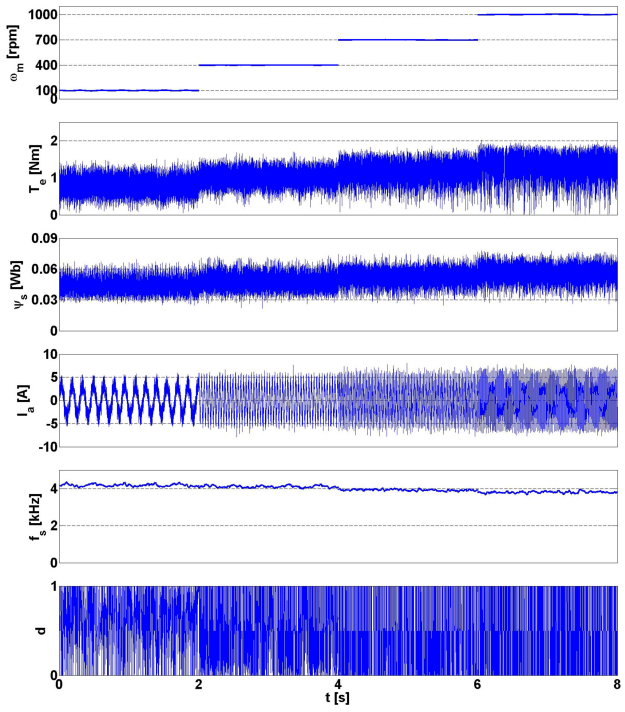

Fig. 7. Experimental results of the conventional DDTC under different speeds. Load: 1 N·m. The graphs are (from top): speed, torque, flux, current of phase A, switching frequency, and duty cycle.

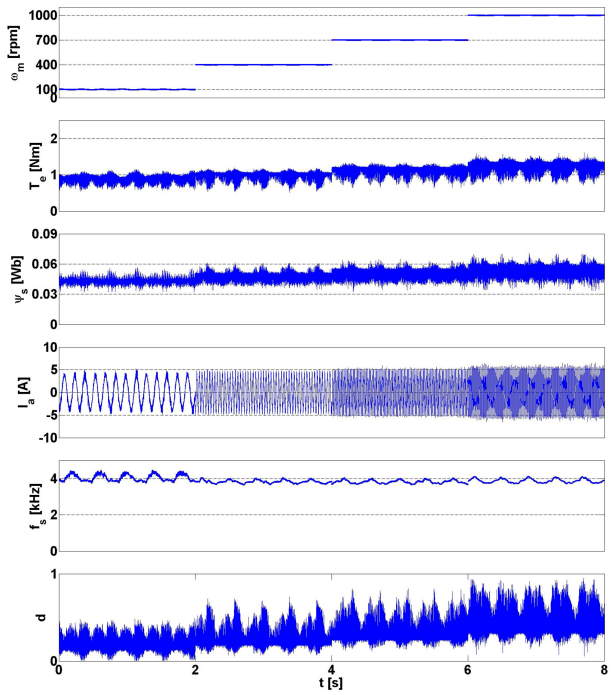

Fig. 8. Experimental results of the proposed DDTC under different speeds. Load: 1 N·m. The graphs are (from top): speed, torque, flux, current of phase A, switching frequency, and duty cycle.

TABLE III
EXPERIMENTAL RESULTS OF CONVENTIONAL AND PROPOSED DDTC UNDER DIFFERENT SPEEDS

	ω_m [rpm]	methods	
		Conventional DDTC	Proposed DDTC
T_{rip} [Nm]	100	0.2262	0.0879
	400	0.2053	0.0924
	700	0.2561	0.0922
	1000	0.339	0.1222
ψ_{rip} [Wb]	100	0.0067	0.0029
	400	0.0064	0.0037
	700	0.0067	0.0046
	1000	0.0077	0.0054
f_s [kHz]	100	4.177	4.063
	400	4.115	3.851
	700	3.921	3.838
	1000	3.896	3.886

two control methods. It can be found in the figures and table that the torque ripple and flux ripple increase with the increasing of speed for both conventional and proposed DDTC, while the torque ripple and flux ripple of the proposed DDTC are consistently lower than that of conventional DDTC. For the switching frequency, there are no obvious variation with the speed increasing for both methods, but the switching frequency of the proposed DDTC is slightly lower than that of the conventional DDTC within the test speed range. For the duty cycle waveforms, the duty cycle of conventional DDTC is unstable over the entire test speed range, while the duty cycle of the proposed DDTC is stable and maintained within a certain range even if more oscillation appears with the speed increasing.

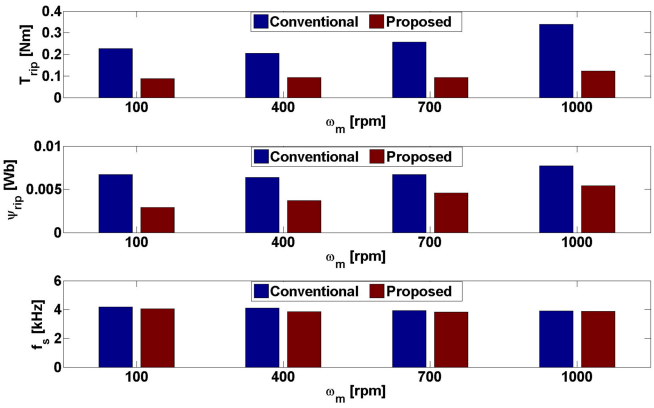

Fig. 9. Experimental results of the conventional and proposed DDTC under different speeds.

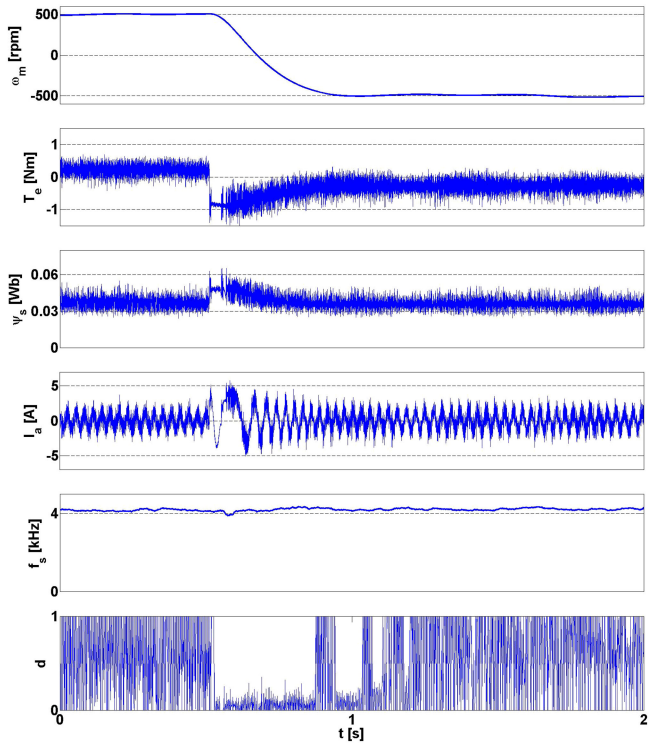

Fig. 10. Dynamic response of the conventional DDTC. The graphs are (from top): speed, torque, flux, current of phase A, switching frequency, and duty cycle.

It can be concluded from the above steady-state experimental results that the proposed DDTC is a an effective control method, and it shows superior steady-state control performance than the conventional DDTC in terms of torque ripple, flux ripple, switching frequency, and current THD, while the computational burden of the proposed DDTC is significantly reduced compared with that of conventional DDTC.

B. Dynamic Response

Apart from steady-state tests, the dynamic responses of these two methods are also tested and compared. Figs. 10 and 11 are the dynamic responses of the conventional DDTC and proposed DDTC, respectively. The mechanical speed changes from 500 to −500 r/min without load. The experimental waveforms show that both methods can track the command speed and reach the reference speed in a short time, and there is no obvious difference between these two methods in dynamic response time. It can be stated that the quick dynamic response is retained in the proposed DDTC, while the algorithm complexity is significantly reduced.

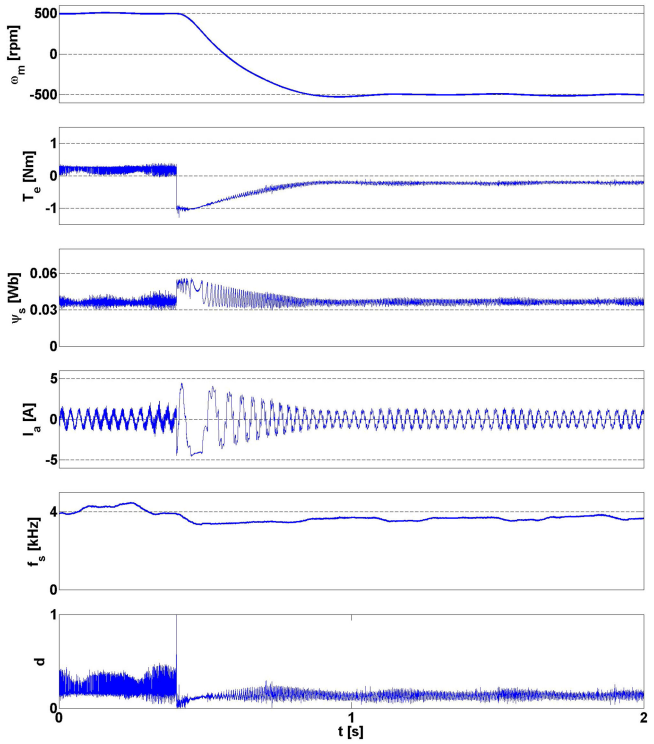

Fig. 11. Dynamic response of the proposed DDTC. The graphs are (from top): speed, torque, flux, current of phase A, switching frequency, and duty cycle.

V. Conclusion

This paper proposes a simple and practical DDTC for PMSMs to avoid the complex calculation process associated with conventional DDTC. The implementation process of the proposed DDTC is illustrated in details and the detailed design process of duty cycle generator is presented. The effectiveness and superiority of the proposed DDTC is verified through experimental results. Generally speaking, in both steady-state and dynamic operations, the proposed DDTC shows better control performance than the conventional DDTC, especially in terms of torque ripple and flux ripple. And the computational burden of the proposed DDTC is significantly reduced compared with that of the conventional DDTC, which makes the proposed DDTC more suitable for practical applications.

References

[1] I. Takahashi and T. Noguchi, "A new quick-response and high-efficiency control strategy of an induction motor," *IEEE Trans. Ind. Appl.*, vol. IA-22, no. 5, pp. 820–827, Sep. 1986.

[2] M. Depenbrock, "Direct self-control (DSC) of inverter-fed induction machine," *IEEE Trans. Power Electron.*, vol. 3, no. 4, pp. 420–429, Oct. 1988.

[3] G. S. Buja and M. P. Kazmierkowski, "Direct torque control of PWM inverter-fed AC motors—A survey," *IEEE Trans. Ind. Electron.*, vol. 51, no. 4, pp. 744–757, Aug. 2004.
[4] S. Payami and R. K. Behera, "An improved DTC technique for low-speed operation of a five-phase induction motor," *IEEE Trans. Ind. Electron.*, vol. 64, no. 5, pp. 3513–3523, Jan. 2017.
[5] A. Shinohara, Y. Inoue, S. Morimoto, and M. Sanada, "Maximum torque per ampere control in stator flux linkage synchronous frame for DTC-based PMSM drives without q-axis inductance," *IEEE Trans. Ind. Appl.*, vol. 53, no. 4, pp. 3663–3671, Jul./Aug. 2017.
[6] A. Rajaei, M. Mohamadian, and A. Y. Varjani, "Vienna-rectifier-based direct torque control of PMSG for wind energy application," *IEEE Trans. Ind. Electron.*, vol. 60, no. 7, pp. 2919–2929, Jul. 2013.
[7] M. Abdellatif, M. Debbou, I. Slama-Belkhodja, and M. Pietrzak-David, "Simple low-speed sensorless dual DTC for double fed induction machine drive," *IEEE Trans. Ind. Electron.*, vol. 61, no. 8, pp. 3915–3922, Aug. 2014.
[8] T. G. Habetler, F. Profumo, M. Pastorelli, and L. M. Tolbert, "Direct torque control of induction machines using space vector modulation," *IEEE Trans. Ind. Appl.*, vol. 28, no. 5, pp. 1045–1053, Sep./Oct. 1992.
[9] F. Niu, B. Wang, A. S. Babel, K. Li, and E. G. Strangas, "Comparative evaluation of direct torque control strategies for permanent magnet synchronous machines," *IEEE Trans. Power Electron.*, vol. 31, no. 2, pp. 1408–1424, Feb. 2016.
[10] J.-K. Kang and S.-K. Sul, "New direct toque control of induction motor for minimum torque ripple and constant switching frequency," *IEEE Trans. Ind. Appl.*, vol. 35, no. 5, pp. 1076–1082, Sep./Oct. 1999.
[11] K.-B. Lee, J.-H. Song, I. Choy, and J.-Y. Yoo, "Torque ripple reduction in DTC of induction motor driven by three-level inverter with low switching frequency," *IEEE Trans. Power Electron.*, vol. 17, no. 2, pp. 255–264, Mar. 2002.
[12] K.-K. Shyu, J.-K. Lin, V.-T. Pham, M.-J. Yang, and T.-W. Wang, "Global minimum torque ripple design for direct torque control of induction motor drives," *IEEE Trans. Ind. Electron.*, vol. 57, no. 9, pp. 3148–3156, Sep. 2010.
[13] Y. Ren, Z. Zhu, and J. Liu, "Direct torque control of permanent-magnet synchronous machine drives with a simple duty ratio regulator," *IEEE Trans. Ind. Electron.*, vol. 61, no. 10, pp. 5249–5258, Oct. 2014.
[14] F. Niu, Y. Wang, and K. Li, "Direct Torque control for permanent magnet synchronous machines based on duty ratio modulation," *IEEE Trans. Ind. Electron.*, vol. 62, no. 10, pp. 6160–6170, Oct. 2015.
[15] D. Mohan, X. Zhang, and G. H. B. Foo, "A simple duty cycle control strategy to reduce torque ripples and improve low-speed performance of a three-level inverter fed DTC IPMSM drive," *IEEE Trans. Ind. Electron.*, vol. 64, no. 4, pp. 2709–2721, Apr. 2017.
[16] Y. Zhang, Y. Bai, and H. Yang, "A universal multiple-vector-based model predictive control of induction motor drives," *IEEE Trans. Power Electron.*, vol. 33, no. 8, pp. 6957–6969, Aug. 2018.
[17] Y. Zhang, C. Qu, and J. Gao, "Performance improvement of direct power control of PWM rectifier under unbalanced network," *IEEE Trans. Power Electron.*, vol. 32, no. 3, pp. 2319–2328, Mar. 2017.
[18] Y. Zhang, Y. Peng, and H. Yang, "Performance improvement of two-vectors-based model predictive control of PWM rectifier," *IEEE Trans. Power Electron.*, vol. 31, no. 8, pp. 6016–6030, Aug. 2016.
[19] Y. Zhang and H. Yang, "Two-vector-based model predictive torque control without weighting factors for induction motor drives," *IEEE Trans. Power Electron.*, vol. 31, no. 2, pp. 1381–1390, Feb. 2016.
[20] Y. Zhang and H. Yang, "Model-predictive flux control of induction motor drives with switching instant optimization," *IEEE Trans. Energy Convers.*, vol. 30, no. 3, pp. 1113–1122, Sep. 2015.

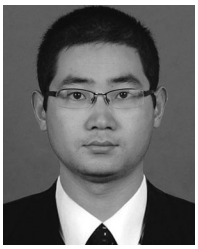

Feng Niu (M'15) was born in Hebei, China, in 1986. He received the B.S. and Ph.D. degrees from Hebei University of Technology, Tianjin, China, in 2009 and 2015, respectively, both in electrical engineering.

He is currently a Postdoctoral Research Fellow with the College of Electrical Engineering, Zhejiang University, Hangzhou, China. From September 2012 to September 2014, he was a Research Fellow with the Electrical Machines and Drives Laboratory, Michigan State University, East Lansing, MI, USA. He has coauthored more than 30 technical articles. His research interests include motor system and control, power converter control, and intelligent electrical equipment.

Xiaoyan Huang (M'09) received the B.E. degree in control measurement techniques and instrumentation from Zhejiang University, Hangzhou, China, in 2003, and received the Ph.D. degree in electrical machines and drives from the University of Nottingham, Nottingham, U.K., in 2008.

From 2008 to 2009, she was a Research Fellow with the University of Nottingham. She is currently a Professor with the College of Electrical Engineering, Zhejiang University, where she is working on electrical machines and drives. Her research interests include PM machines and drives for aerospace and traction applications, and generator system for urban networks.

Leijiao Ge received the Ph.D. degree in electrical engineering from Tianjin University, Tianjin, China, in 2016.

He is currently a Lecturer with the School of Electrical Information and Engineering, Tianjin University. His main research interests include smart grid, cloud computing, and big data.

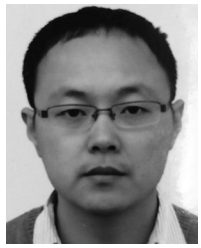

Jian Zhang received the Ph.D. degree in mechanical engineering from Zhejiang University, Hangzhou, China, in 2010.

He is currently an Associate Professor with the College of Electrical Engineering, Zhejiang University. His current research interests include motor design and control and reliability analysis of aero motors.

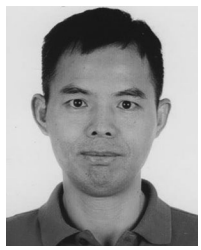

Lijian Wu (M'11–SM'14) received the B.Eng. and M.Sc. degrees from the Hefei University of Technology, Hefei, China, in 2001 and 2004, respectively, and the Ph.D degree from the University of Sheffield, Sheffield, U.K., in 2011, all in electrical engineering.

From 2004 to 2007, he was an Engineer with Delta Electronics (Shanghai) Co, Ltd. From 2012 to 2013, he was with Sheffield Siemens Wind Power Research Center as a Design Engineer, focusing on wind power generators. From 2013 to 2016, he was an Advanced Engineer with Siemens Wind Power A/S in Denmark. In 2016, he joined the College of Electrical Engineering, Zhejiang University, Hangzhou, China, where he is currently a Professor. His current major research interests include design and control of permanent magnet machines.

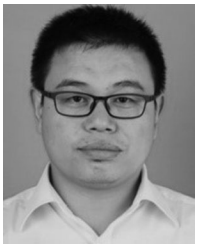

Yao Wang (M'16) was born in Hebei, China, in 1981. He received the B.S., M.S., and Ph.D. degrees from the Hebei University of Technology, Tianjin, China, in 2006, 2009, and 2012, respectively, all in electrical engineering.

He is currently an Associate Professor with the School of Electrical Engineering, Hebei University of Technology. He has coauthored more than 20 technical articles. His research interests include intellectualization of electrical apparatus and fault detection and mitigation for microgrid.

Kui Li was born in Hebei, China, in 1965. He received the B.S. and M.S. degrees from the Hebei University of Technology, Tianjin, China, in 1987 and 1992, respectively, and the Ph.D. degree from Fuzhou University, Fuzhou, China, in 1996, all in electrical engineering.

He is currently a Professor with the School of Electrical Engineering, Hebei University of Technology. He has coauthored more than 100 technical articles and two monographs. His research interests include reliability and intellectualization of electrical apparatus, fault diagnosis, and life prediction of electrical apparatus.

Youtong Fang (M'11–SM'15) received the B.S. and Ph.D. degrees in electrical engineering from Hebei University of Technology, Hebei, China, in 1984 and 2001, respectively.

He is currently a Professor with the College of Electrical Engineering, Zhejiang University, Hangzhou, China. His research interests include the application, control, and design of electrical machines.